
Forest tree species classification and entropy-derived uncertainty mapping using extreme gradient boosting and Sentinel-1/2 data

Abdulhakim M. Abdi * and Fan Wang

Centre for Environmental and Climate Science (CEC), Lund University, Sweden

* Correspondence: hakim.abdi@cec.lu.se

Abstract

We present a wall-to-wall map of dominant tree species in Swedish forests accompanied by pixel-level uncertainty estimates. The tree species classification is based on spatiotemporal metrics derived from Sentinel-1 and Sentinel-2 satellite data, combined with field observations from the Swedish National Forest Inventory and auxiliary data on geomorphometry and canopy height. We apply an extreme gradient boosting model with Bayesian optimization to relate field observations to satellite-derived features and generate the final species map. Classification uncertainty is quantified using Shannon's entropy of the predicted class probabilities, which provide a spatially explicit measure of model confidence. The final model achieved an overall accuracy of 85% (F1 score = 0.82, Matthews correlation coefficient = 0.81), and mapped species distributions showed strong agreement with official forest statistics ($r = 0.96$). Variable importance analysis revealed that the most influential predictors were optical bands from Sentinel-2, particularly those acquired in spring and summer. This study provides scalable, interpretable, and policy-relevant method for tree species mapping with integrated uncertainty that are well-suited to meet emerging legislative and environmental goals.

Introduction

Forests are critical carbon sinks that help mitigate climate change by absorbing greenhouse gases from the atmosphere (Pan et al. 2024). They are essential for maintaining biodiversity by providing habitats for a myriad of organisms from higher plants and animals to fungi and microorganisms (Peh, Corlett, and Bergeron 2025). Additionally, forests support human livelihoods by supplying resources such as timber, food, and medicinal products (Dlamini 2019), while also regulating water cycles and preventing soil erosion (Creed et al. 2016). Sustainable forest management practices are essential to maintain these ecosystems' health and productivity, ensuring that they continue to provide these services.

Understanding the composition of tree species within forests is fundamental to managing them sustainably as different species contribute uniquely to ecosystem functions and resilience. For instance, forests with diverse tree species have been shown to enhance ecosystem productivity and stability (Morin et al. 2018; Morin et al. 2011), which are important for biodiversity conservation (Liang et al. 2016). Moreover, the selection of appropriate tree species is an important forest management decision that can affect the forest microclimate (Zhang, Landuyt, et al. 2022) and soil carbon sequestration (Liu et al. 2018). Therefore, information on the distribution of tree species within forests is essential for conserving these ecosystems and maintaining the services they provide.

Sweden has the largest forest area in the European Union (EU), covering approximately 280,000 km², or approximately 70% of its land area (Roberge et al. 2020). Forests are an integral part of Sweden's economy, providing resources such as timber and non-timber products that make it the world's third-largest exporter of coniferous sawn wood and second-largest exporter of pulp and paper (Roberge et al. 2020). Ninety-two percent (92%) of the standing timber in Swedish forests comprises of just three dominant species – Norway spruce (*Picea abies*, 40.3%), Scots pine (*Pinus sylvestris*, 39.3%), and Birch (*Betula spp.*, 12.4%). Although Sweden covers a wide biogeography, ranging from boreal to nemoral/continental (Preislerová et al. 2024), the dominance of these three species is high in northern parts of the country (97%) and low southern parts (86%). Thus, the highest levels of tree diversity occur in southern Sweden (Göteborg, Figure 1) where most of the deciduous forests comprise Oak (*Quercus spp.*), Beech (*Fagus sylvatica*), and other nemoral broadleaved trees (Roberge et al. 2020).

The National Forest Inventory (NFI) of Sweden serves as a primary source for deriving statistics on forest resources at both national and subregional scales (Fridman and Westerlund 2016). The inventory area is divided into geographic strata to ensure adequate representation of different forest types, land uses, and regions. Despite its extensive geographic coverage, the NFI has two drawbacks that limit its utility for detailed geospatial analysis – it is based on a sample plot design, which prevents a spatially continuous depiction of forests, and it is conducted over a multi-year sampling interval due to the extensive areal coverage. Furthermore, the coordinates of the sample plots are not publicly shared to avoid the risk of human disturbances that could compromise their representativeness (Schadauer et al. 2024). These limitations necessitate the use of complementary methods that can be deployed in a timely manner to efficiently map Swedish forests, such as Earth observation technology.

The European Commission's recent proposal for a Forest Monitoring Law (European Commission 2023) reflects a shift towards coordinated data-driven forest governance that prioritises timely, spatially explicit information. The proposed

legislation responds to a growing recognition that existing field-based forest monitoring practices across member states are in and of themselves insufficient for addressing rapid changes driven by climate stressors, biodiversity loss, and increased harvesting pressure (Atzberger et al. 2020; European Commission 2021; Raši 2020). Key components of the proposal include the development of digital forest maps, timely reporting on forest disturbances, and the integration of Earth observation into national monitoring frameworks. This marks a shift towards data-driven approaches to forest governance in Europe and emphasises the need for scalable remote sensing workflows that complement and enhance national forest inventories. In this context, Sweden's long-standing reliance on sample-based inventories and its extensive forest cover make it a relevant case study for demonstrating how satellite-derived species mapping can help meet emerging legislative and policy demands.

Earth observation technology provides valuable tools that help address the challenges of large-scale forest mapping. In Canada, studies have directly examined the integration of satellite data with the country's National Forest Inventory. For example, Wulder et al. (2020) developed a national-scale method to map forest area using Landsat time series and NFI reference plots. Hermosilla et al. (2022) mapped the distributions of 37 tree species across Canada's forests using a harmonised Earth observation framework, again validating these results against NFI data. These studies highlight the potential of satellite remote sensing to complement, rather than replace, field-based forest inventories, especially in areas where plot networks are sparse or where rapid updates are required for monitoring forest dynamics under climate or land use change.

In recent years, two key satellite systems have emerged as essential resources for this purpose: Sentinel-1, which carries the C-band synthetic aperture radar (SAR) and Sentinel-2, which carries the optical Multispectral Instrument (MSI). The Sentinel-2 pair of satellites (A and B) offer improved spatial and temporal resolution with a revisit interval of five days and a spatial resolution ranging from 10 to 60 meters. These instruments have high thematic accuracy for tree cover mapping (Ottosen et al. 2020) and have proven

effective in distinguishing tree species across different European ecosystems (Hemmerling, Pflugmacher, and Hostert 2021; Grabska, Frantz, and Ostapowicz 2020; Persson, Lindberg, and Reese 2018; Grabska et al. 2019) due to the red-edge bands and the higher revisit interval that enhances phenological distinction between species (Persson, Lindberg, and Reese 2018), among other aspects. The Sentinel-1 pair (A and B) combines high spatial resolution (5–20 meters) and 6-day revisits, which is unparalleled among currently operational SAR satellite systems. However, the mission of Sentinel-1B ended in December 2021 after problems arose with the power supply that prevented the satellite from delivering data. Its replacement (Sentinel-1C) was successfully launched in December 2024. Sentinel-1 has also been effectively utilised for forest type and tree species classification (Udali, Lingua, and Persson 2021; Dostálová et al. 2018; Dostálová et al. 2021) due to SAR backscatter sensitivity to canopy structure and geometry (Rignot et al. 1994; Varghese and Joshi 2015; Varghese, Suryavanshi, and Joshi 2016). Consequently, the integration Sentinel-1 and Sentinel-2 has enabled the detection of distinct, and complementary, properties of the tree canopy (Lechner et al. 2022; Bjerreskov, Nord-Larsen, and Fensholt 2021; Blickensdörfer et al. 2024; Mngadi et al. 2021).

The availability of Earth observation data on cloud platforms such as Microsoft Planetary Computer and Google Earth Engine (GEE) (Gorelick et al. 2017), enhancing the signal-to-noise ratio by combining several multitemporal images becomes a crucial step. Spectral-temporal metrics (STMs) based on satellite image composition transform multiple images from a specific time frame (such as seasonal or annual) into a single composite image. Each pixel in the composite reflects the combined properties of the corresponding pixel

Study Area

The study area encompasses most of the historical region of Götaland (Figure 1 a) and includes six administrative counties (Figure 1 b) that altogether cover 55,000 km² and comprise 26% of the country's population. Fifty-seven percent (57%) of the area is classified as productive forest (Figure 1 c), which, according to Sweden's Forestry Act

stack based on statistical summaries (e.g., mean, standard deviation, maximum, minimum or specific percentiles) during the chosen period. This approach has been successfully implemented in the large-scale mapping of various forest tree species (Grabska-Szwagrzyk et al. 2024; Blickensdörfer et al. 2024). Building on these advancements, the current state-of-the-art utilises advanced machine learning algorithms to extract and interpret signals specific to different tree species from Earth observation data.

In this study, we classify and estimate the mapped uncertainty of seven tree species (Table 1), which represent 97% of all the trees species recorded in Swedish forests, at a spatial resolution of 10 meters. The main objectives of the study are to evaluate the potential of Sentinel-1/2 observations, including spectral bands, polarization channels, vegetation indices, and STMs for predicting tree species, and assess the influence of geomorphometry (slope, aspect, elevation, topographic wetness) and canopy height on their spatial distribution. Data for training, testing and validation were derived from the Swedish NFI, and the importance of the predictors were assessed. Extreme gradient boosting (Chen and Guestrin 2016) with Bayesian optimization was chosen to model the distribution of tree species, and an uncertainty map of model predictions based on Shannon's entropy (Wang 2008) was also produced. The resultant tree species maps were compared to official published forest statistics for the study area (Riksskogstaxeringen 2024). Our goal is to provide not only accurate tree species predictions but also a robust framework for interpreting model confidence at the pixel level, which is an essential step toward operational forest monitoring that is both scientifically robust and policy relevant.

refers to any forested land capable of generating an average of at least one cubic meter of timber per hectare annually (Riksdag 1979). The area comprises hemiboreal and nemoral ecological zones and therefore exhibits a transition from the conifer-dominated characteristics of boreal systems to the broadleaf-rich landscapes of temperate zones (Roberge et al. 2020). In northern parts of the study area boreal conifers such as Norway spruce (*Picea*

abies) and Scots pine (*Pinus sylvestris*) remain dominant but are interspersed with temperate deciduous species like birch (*Betula spp.*) and alder (*Alnus spp.*). These mixed forests represent a gradual transition, where the colder, conifer-reliant ecosystems of the north give way to forests with a higher proportion of temperate broadleaf species in the south. In the southernmost nemoral zones,

broadleaf deciduous species such as oak (*Quercus robur*) and beech (*Fagus sylvatica*) become more prominent and often form contiguous forests. This combination results in the study area having a rich mosaic of forest types that blends northern boreal characteristics with elements of temperate deciduous forests.

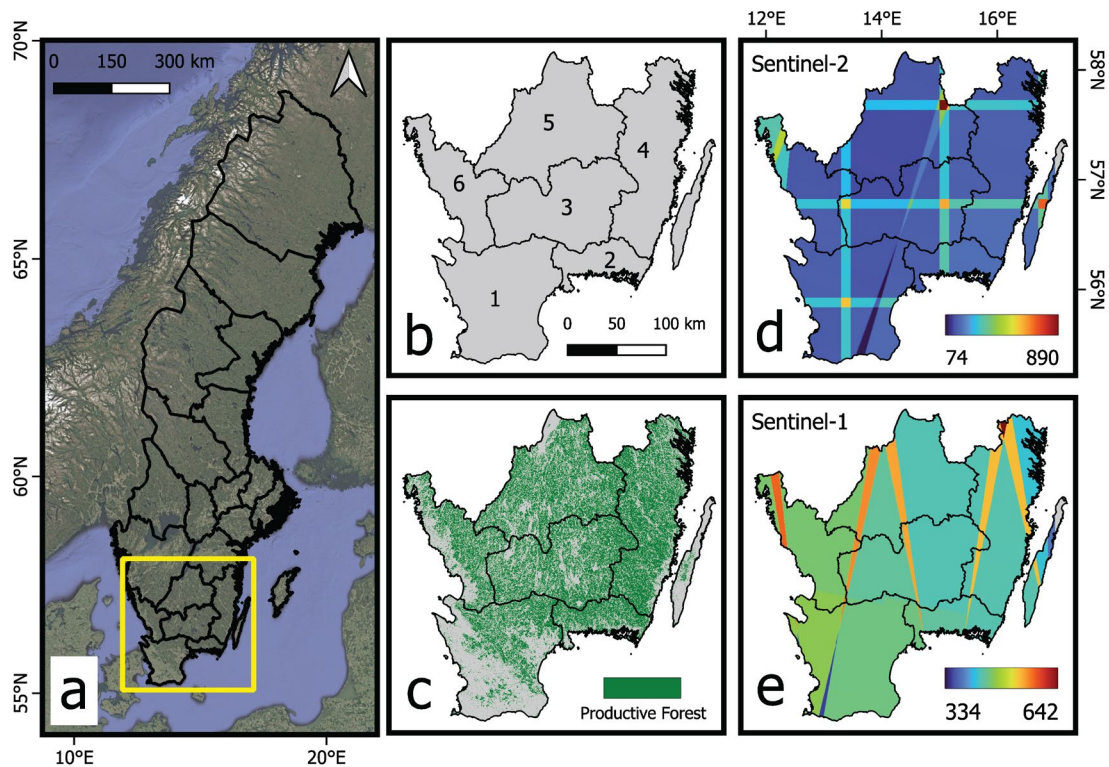


Figure 1. The study area in southern Sweden (a) is composed of six counties (*län*) (b) – Skåne (b1), Blekinge (b2), Kronoberg (b3), Kalmar (b4), Jönköping (b5), and Halland (b6) – and most of it is classified as productive forest (c). The final two panels display the coverage of satellite observations between 2021 and 2023 for Sentinel-2 MSI with less than 70% cloud cover (d) and Sentinel-1 SAR in both orbital directions (e).

Data

Swedish National Forest Inventory

The Swedish National Forest Inventory (NFI) employs probability sampling through a stratified cluster design. Groups of 4 to 12 sample plots, arranged in square or rectangular patterns called tracts, are systematically distributed across the country (Fridman and Westerlund 2016; Fridman et al. 2014). Of these plots, 60% are permanent and revisited on a five-year rotation, while the remaining 40% are temporary and measured only once to enhance spatial coverage. Permanent plots

have an area of 314.16 m² ($r=10$ m) (Figure 2 a), while temporary plots have an area 153.94 m² ($r=7$ m) (Figure 2 b). The side lengths of tracts vary depending on location (Figure 2 c). Within the study area, the sides of the tracts are approximately 300 m in the south, increasing to 800 m in the north (reaching 1800 m in the far north of Sweden). Similarly, the spacing between individual plots within tracts varies geographically, starting at 300 m in the south and increasing to 600 m in the north (extending to 800 in the far north of Sweden). Currently, the total sample includes 4,500 permanent tracts and 2,500 temporary tracts (Lundström and Wikberg 2017). Approximately one-fifth of these tracts are surveyed each year,

resulting in the measurement of around 12,000 plots annually. All trees that have a diameter of 100 mm or more within each plot are measured at breast height (DBH, 1.3 m above ground). Trees with DBH between 40 and 100 mm, and those less than 40 mm are measured in subplots (with radii of 3.5 m and 1 m, respectively) within permanent and

temporary plots. A subset of sample trees is then chosen with a probability proportional to their basal area at breast height. For these selected sample trees, species and tree class are recorded, and their total height is measured.

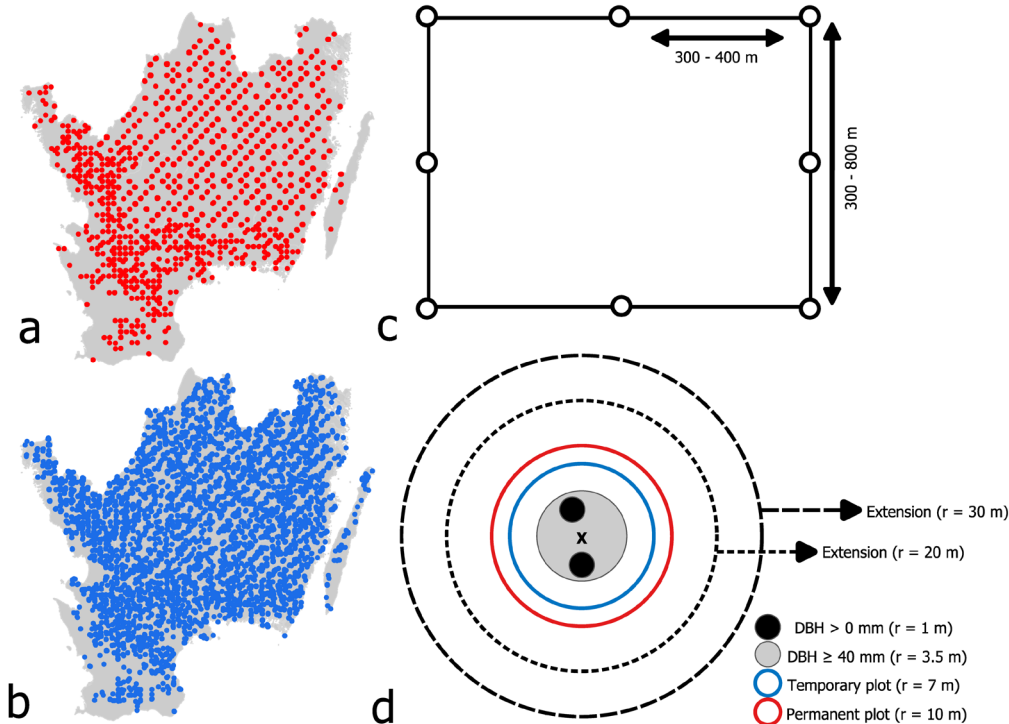


Figure 2. Spatial distribution of the permanent (a) and temporary tracts (b) in the study area. Note that the sampling density is greater in the southernmost parts of the study area compared to the northern parts. Each tract takes a square or rectangular shape (c) that comprises 4 to 12 plots that are spaced at varying distances. Trees with a diameter of ≥ 100 mm are measured at breast height (1.3 m), while those with diameters of 40–100 mm and < 40 mm are measured in subplots with radii of 3.5 m and 1 m, respectively, within both permanent and temporary plots (d). The extensions around the plots ($r = 20$ m and $r = 30$ m) were manually created to expand the sample size of the Sentinel-1 and Sentinel-2 pixels used to train the machine learning model.

Satellite observations

Sentinel-1 Synthetic Aperture Radar (SAR)

The Sentinel-1 Level-1 Ground Range Detected (GRD) product was used in this study. This dataset has been processed to backscatter coefficients (σ^0), which represent radar cross-section per unit ground area, and converted to decibels (dB) using the formula $10 \cdot \log_{10}(\sigma^0)$ to account for the wide variation in backscatter intensity. Radiometric calibration was applied using sensor parameters in the GRD metadata to compute backscatter intensity. Orthorectification was performed using a digital elevation model to convert ground range geometry into terrain-corrected backscatter

coefficients. The data was post-processed into analysis-ready data (Mullissa et al. 2021), incorporating border noise correction, speckle filtering, and radiometric terrain normalization. The Interferometric Wide Swath (IW) acquisition mode was used with dual polarization, VV (vertical transmit, vertical receive) and VH (vertical transmit, horizontal receive). A total of 1,317 Sentinel-1 acquisitions were processed in GEE.

Sentinel-2 Multispectral Imager (MSI)

The Harmonised Sentinel-2 Surface Reflectance (L2A) product was used in this study. These data were orthorectified in Sen2Cor (Louis et al. 2016) to correct geometric distortions caused by terrain variations and sensor angles, and atmospheric

correction was applied (Louis and L2A Team 2021). Additionally, the scene classification module in Sen2Cor was used to identify low-quality pixels, generating a scene classification map to distinguish between clouds and snow during the atmospheric correction process. Sentinel-2 data are provided in three spatial resolutions – 10 m, 20 m, 60 m – and thirteen spectral bands. Ten of these bands – blue (B2), green (B3), red (B4), red-edge (B5, B6, B7), near-infrared (B8, B8A), and shortwave-infrared bands (B11, B12) – were used in this study. The remaining three bands (B1, B9, B10) are used primarily for atmospheric correction and water vapor analysis and were therefore not included in the analysis. Scenes with cloud cover $\leq 70\%$ were chosen to exclude images that are more prone to geometric errors (Laurin et al. 2022; White et al. 2014). The Sentinel-2 scenes that met the criteria numbered 2,746 and were processed in GEE.

Auxiliary Variables

Geomorphometry influences the distribution of tree species by controlling soil properties and hydrological conditions at the landscape scale. Digital elevation models (DEMs) are essential for deriving geomorphometric features like the slope and topographic wetness index (TWI, $\ln(a/\tan\beta)$), which have been shown to influence organic layer thickness, soil pH, and nutrient distribution (Seibert, Stendahl, and Sørensen 2007). To characterise the topography of the study area, FABDEM v 1-2 (Forest And Buildings removed Copernicus DEM) (Hawker et al. 2022) was used to extract elevation, slope, aspect, and TWI in the study area. This dataset overall outperforms other large-scale DEMs (Osama, Shao, and Freeshah 2023), especially in forested areas (Huang and Yang 2025; Marsh, Harder, and Pomeroy 2023). FABDEM was resampled from 30 m to 10 m to match the spatial resolution of the other datasets in this study.

Forest canopy height is intrinsically linked to the dominant tree species as it reflects the structural attributes of forest ecosystems (Besic et al. 2025), which are strongly influenced by species-specific growth patterns and ecological strategies. The maximum size of a tree, including its height, has been shown to correlate with tree species diversity (Hakkenberg et al. 2016) because different species

occupy specific vertical niches within the forest (Farhadur Rahman, Onoda, and Kitajima 2022), competing for resources such as light. The observation that dominant tree species significantly affect variations in canopy height highlights how certain species, such as Norway spruce, can shape canopy structure. The canopy height map used here was developed by Lang et al. (2023) using a combination of deep convolutional neural network model and relative height profiles from the Global Ecosystem Dynamics Investigation (GEDI) spaceborne lidar (Dubayah et al. 2020). The spatial resolution of this dataset (10 m) allows for greater spatial precision, which may explain its stronger alignment with data from airborne laser scanning (Torresani et al. 2023). This resolution enhances the ability to capture height variability, which has been shown to correlate closely with tree species diversity (Torresani et al. 2020).

Methods

Data preparation

NFI Data

The NFI dataset used in this study had 23,138 plots encompassing the period 1996 – 2023. The dataset contained duplicates from different sampling years and no-data values where species proportions could not be determined. To prepare the data, no-data values were removed, and duplicates were resolved by retaining only the most recent inventory record. Plots that were disturbed by clearcuts (either inside or within a 10 m buffer) were removed by performing spatial and temporal comparisons using the latest version of the Swedish Forest Agency’s clearcut database. Plots that were sampled after the most recently recorded clearcut with a mean tree height exceeding 5 meters were kept in order to meet the definition of forest land under the Swedish Forestry Act (Riksdag 1979). Only pure-stand plots were used to maintain species representation and minimise reference data location errors. A threshold of 80% (Blickensdörfer et al. 2024; Welle et al. 2022) was applied to differentiate between pure- and mixed-stands – therefore if any tree species constituted 80% or more of the composition in a sampling plot, it was classified as a pure-stand plot with that species as the dominant one. This procedure yielded a final

dataset of 6,527 plots that was used for further analysis (Table 1).

Preliminary testing indicated that the number of plots was insufficient to produce robust results for some of the deciduous species. To increase the sample size for rarer tree species, plots where these species were dominant were expanded to areas of 1,256.64 m² ($r = 20$ m) and 2,827.43 m² ($r = 30$ m) to include additional Sentinel-1 and Sentinel-2 pixels for training the machine learning algorithm to better distinguish these species (Figure 2 d). We

performed this expansion through manual interpretation of 1,568 plots using publicly available multitemporal high-resolution orthophotos from Google Earth and Google Street View photographs for plots near public roads. Plots dominated by species other than Norway spruce or Scots pine were selected for interpretation. For each plot, we determined whether the radius could be expanded to 20 m or 30 m based on the conditions within the original plot.

Table 1. Summary of the Swedish NFI data (mean \pm standard deviation). The samples column represents the number of 10 m pixels extracted from the plot following the expansion procedure (see Methods section).

Species	Stand Age (Years)	Diameter at breast height, DBH (mm)	Volume (m ³ ha ⁻¹)	Height (m)	Plots	Samples
Scots pine <i>Pinus sylvestris</i>	65 \pm 39	234 \pm 97	136 \pm 94	14 \pm 6	2209	4081
Norway spruce <i>Picea abies</i>	42 \pm 25	197 \pm 92	197 \pm 152	16 \pm 7	2750	5197
Birch <i>Betula spp.</i>	29 \pm 23	135 \pm 100	70 \pm 61	10 \pm 7	754	5421
Oak <i>Quercus robur</i>	72 \pm 42	334 \pm 179	157 \pm 140	15 \pm 8	210	2348
Alder <i>Alnus spp.</i>	50 \pm 27	242 \pm 102	199 \pm 174	15 \pm 7	135	1028
Beech <i>Fagus sylvatica</i>	84 \pm 35	387 \pm 166	256 \pm 197	21 \pm 7	287	5199
Aspen <i>Populus spp.</i>	37 \pm 33	195 \pm 158	143 \pm 110	12 \pm 10	46	203
Other species <i>Other spp.</i>	41 \pm 35	208 \pm 132	92 \pm 91	12 \pm 9	136	661

Satellite and auxiliary Data

In addition to the raw Sentinel-1 backscatter and Sentinel-2 reflectance, several vegetation indices were derived from them to enhance the discrimination of tree species by capturing key biophysical and phenological characteristics of forest stands. These include the dual-polarization

radar vegetation index (Nasirzadehdizaji et al. 2019) (Equation 1), cross-ratio index (Vreugdenhil et al. 2020) (Equation 2), enhanced vegetation index (Huete et al. 2002) (Equation 3), and the multispectral ratio vegetation index (Pearson and Miller 1972) (Equation 4). Three-month seasonal composites (using the median value) were generated for the years 2021 to 2023,

corresponding to the four seasons: DJF (December–February), MAM (March–May), JJA (June–August), and SON (September–November). A key advantage of using seasonal image composites to extract STMs is that processing time is significantly reduced, and the composites effectively capture forest phenology (Nasiri et al. 2023) while mitigating issues related to cloud cover and snow. This approach resulted in 16 bands and indices \times 12 seasons + 5 static auxiliary layers = 197 features.

$$RVIr = \frac{4\sigma^{oVH}}{(\sigma^{oVV} + \sigma^{oVH})} \quad (1)$$

$$CR = \frac{\sigma^{oVH}}{\sigma^{oVV}} \quad (2)$$

$$EVI = 2.5 \frac{NIR - RED}{NIR + 6 \times RED - 7.5 \times BLUE + 1} \quad (3)$$

$$RVIm = \frac{RED}{NIR} \quad (4)$$

where, VH (vertical transmit, horizontal receive) and VV (vertical transmit, vertical receive) are Sentinel-1 polarizations; σ^o is the backscatter coefficient; BLUE, RED, and NIR are the blue (band 2, 490 nm), red (band 4, 665 nm), and near-infrared (band 8, 842 nm) bands of Sentinel-2.

Machine learning approach

Algorithm choice

The data (NFI+Satellite) was divided into optimization (80%) and validation (20%) subsets. Model training and testing was done on optimization subset, and final evaluation was done on the independent validation dataset. We initially compared four machine learning models: one-dimensional convolutional neural network (1D-CNN), support vector machines (SVM), random forest (RF), and extreme gradient boosting (XGB). The evaluation metrics selected were model overall accuracy (OA), model F1 score, model precision, model recall (F1, precision, and recall were averaged unweighted across classes), and the F1 score per class ($F1_{class}$). XGB produced the best results ($F1 = 0.83$, $OA = 85\%$) during the model optimization and was thus chosen to perform the tree species classification.

Class imbalance

The final dataset yielded 24,138 sample pixels, which were highly imbalanced (Table 1). An imbalanced dataset causes multi-class classification to be biased toward the majority classes, leading to poor prediction accuracy for underrepresented classes. This happens because the model prioritises minimizing overall error rather than learning meaningful patterns from all classes equally (He and Garcia 2009; Fassnacht et al. 2016). We tested three strategies to remedy class imbalance in our analysis: (1) a simple down-sampling of the dataset using the number of aspen pixels (class with least samples) as a reference resulted in an F1 score of 0.67, (2) merging aspen with the ‘other species’ class and then using alder as a baseline to down-sample the dataset yielded a slightly higher F1 Score of 0.76, and (3) assigning class weights inversely proportional to class frequencies (Chen et al. 2025), which produced the best results ($F1 = 0.83$) and was implemented in the workflow.

Data leakage

As machine learning is increasingly being used in ecological remote sensing applications, there is a concern that data leakage (Stock, Gregr, and Chan 2023) could adversely affect the results. This occurs due to the presence of spatial autocorrelation when training and validation data are geographically clustered, causing the model to access information that artificially inflates its accuracy (Ploton et al. 2020). We tested three strategies to limit data leakage in our analysis:

- (1) the commonly used 80/20 split whereby 80% of the data is assigned to the training subset and 20% to the testing subset while preserving class ratios through stratified sampling resulted in an F1 score of 0.93. Since our data consists of pixels extracted from circular plots, training and testing pixels can come from the same plot, leading to data leakage and over-optimistic predictions.
- (2) a group-based split that treats each sampling plot as a distinct group and data from the same plot is never in both training and testing. This approach produced relatively poor results ($F1 = 0.68$) for rarer species such as aspen

because of the paucity of pixels that can be used for training and testing.

- (3) spatial block splitting (Valavi et al. 2019; Roberts et al. 2017) whereby the data are first grouped into blocks of a given size (in meters) and then the blocks are split randomly between training and testing sets. Experiments were conducted using sizes of 60 m (F1 = 0.82), 100 m (F1 = 0.69), 150 m (F1 = 0.71), 200 m (F1 = 0.63). We therefore opted for 60 m blocks to reduce spatial autocorrelation.

Hyperparameter optimization

XGB comprises three categories of configuration parameters: general parameters, booster parameters, and learning task parameters (Chen et al. 2025). In this study, we refer to the subset of these parameters that are subject to tuning as *hyperparameters*. Since we used the tree booster (*gbtree*), which is commonly the default in most applications due to its consistently strong performance, we focused exclusively on tuning booster hyperparameters related to model complexity and training behaviour.

We used a two-stage hyperparameter tuning strategy beginning with an initial broad search followed by more targeted optimization. In the first stage, we adopted a stepwise grid search, evaluating combinations around the default XGB settings. The procedure followed a sequential structure: (1) fixing the learning rate at 0.1 while tuning the number of trees ($n_estimators$); (2) adjusting max_depth and min_child_weight ; (3) modifying min_split_loss ; (4) optimizing $colsample_bytree$ and $subsample$; and (5) tuning the regularization terms reg_alpha and reg_lambda . After narrowing the parameter space, we used Bayesian optimization (scikit-optimize/BayesSearchCV (Head et al. 2021)) in the second stage to further adjust the most influential parameters within the reduced ranges. Additional tuning of other parameters often yielded gains in training performance, but these were accompanied by slight reductions in test accuracy, indicating potential overfitting.

The optimised parameters where: $n_estimators = 3500$; $learning_rate = 0.118914842747$; $colsample_bytree = 0.5$; $min_split_loss = 1e-09$;

$max_depth = 4$; $min_child_weight = 1$; $reg_alpha = 0.001$; $reg_lambda = 0.01$; $subsample = 0.9$.

Although this model showed strong performance, we ultimately used a simpler configuration ($n_estimators = 3000$, $learning_rate = 0.1$) to generate the final maps. This decision was based on slightly better testing accuracy and a conscious effort to reduce model complexity and limit the risk of overfitting.

Variable importance

Variable importance was assessed using total gain, which quantifies the cumulative improvement in the objective function resulting from all splits involving a particular feature across the ensemble of decision trees. Specifically, it sums up the reduction in multiclass log loss achieved at each split where the feature is used. This metric reflects both how often a feature is used in splits and how effective it is in reducing the overall loss, thus presenting a feature’s contribution to the model’s predictive performance (Chen and Guestrin 2016).

Quantifying uncertainty

XGB produces a probability vector for each prediction in a multiclass classification to indicate how likelihood of each class for a given input. In such probability distributions, entropy (also called Shannon’s entropy (Shannon 1948)) provides a more theoretically grounded framework for quantifying uncertainty (Wang 2008). In simple terms, entropy is a measure of disorder or randomness in a system. It quantifies how ‘spread out’ the predictions are. The entropy H of a predicted class probability vector $p = [p_1, p_2, \dots, p_K]$, where K is the number of classes, is calculated as (Equation 5):

$$H_{(p)} = - \sum_{i=1}^K p_i \log(p_i) \quad (5)$$

Then, dividing by the maximum possible entropy, $\log(K)$, normalises the values and ensures values fall between 0 and 1. Entropy values close to 0 indicate high confidence, because most of the probability mass is assigned to a single class. For example, a probability vector that looks like this: [0.93, 0.02, 0.01, 0.00, 0.01, 0.01, 0.02] has very low entropy because the classifier is clearly favouring the first class (0.93) over the others. In

contrast, a vector such as [0.15, 0.14, 0.14, 0.14, 0.14, 0.14, 0.15] distributes probabilities more evenly across all classes, indicating high uncertainty, and consequently high entropy, close to $\log(K)$. Thus, a continuous-valued uncertainty map is generated by applying this entropy calculation to every pixel to accompany the discrete multiclass predictions, which helps highlight model confidence.

Results

Classification performance

The final map (Figure 3 a) based on XGB had an overall accuracy of 85% and a Matthews correlation coefficient of 0.81 based on the independent validation subset. On average, the model achieved a mean recall of 0.80 (± 0.09) and mean precision of 0.84 (± 0.05), with a corresponding F1 score of 0.82 (± 0.07) (Table 2). The average omission error was 0.19, and commission error was 0.15, reflecting relatively balanced misclassification rates across the classes. The 10-fold cross-validation accuracies, which are based on optimization subset, were all above the 0.9 mark: 0.93 ± 0.02 (precision), 0.95 ± 0.03 (recall), and 0.94 ± 0.02 (F1 score). The model also demonstrated strong overall performance on the independent validation subset across most tree species classes, with particularly high scores for dominant species. Beech performed best overall, with the highest recall (0.93) and a strong F1 score of 0.92, indicating that the model reliably identified this species with low omission and commission errors. Two of the most spatially widespread species in Götaland, Norway spruce and Scots pine, showed similarly solid performance, with F1 scores of 0.82 and 0.83 respectively. Birch also stood out with near-identical recall and precision values, reflecting near-equal accuracy in identifying this class. Oak showed a high precision (0.88) and recall (0.86), resulting in an F1 score of 0.87. Aspen had slightly lower recall (0.76) but very high precision (0.92), suggesting it was occasionally missed by the model but almost always correctly classified when predicted. In contrast, alder and ‘other species’ showed the weakest performance as both classes had relatively low recall (0.66 and 0.66, respectively), indicating a higher rate of

omission errors. Alder’s F1 score was 0.72, and ‘other species’ was 0.71 – still reasonably high but notably lower than the other classes, likely due to more heterogeneous or less distinct spectral signatures.

Model uncertainty

Although the mapped entropy-based uncertainty was overall low across the study area (mean = 0.16 ± 0.19 , Figure 3 b), there were notable differences in classification confidence across tree species (Figure 4). Norway spruce, Scots pine, and beech exhibit the lowest median entropy values, indicating that the model consistently assigned these species with high confidence across the study area. These species likely had distinct and stable spectral-temporal signatures, which contributed to more certain predictions. In contrast, species such as aspen, alder, and other species show considerably higher entropy values, reflected by wider interquartile ranges and higher medians. These elevated uncertainty levels suggest greater confusion during classification, likely due to a combination of spectral similarity with other deciduous species, more heterogeneous stand compositions, and lower representation in the training data. The aspen class in particular displays the greatest spread and central tendency in entropy, probably due to the small number of samples in the final dataset (203). The ‘other species’ class has the second-highest uncertainty despite having more than three times the number of samples as aspen (661), and this high uncertainty is consistent with the challenge of lumping diverse minor species into a single group, which reduces the model’s ability to make confident predictions. Intermediate uncertainty is observed for birch and oak, which show moderate median entropy values. Although generally well-classified based on performance metrics, these species may exhibit spectral overlap with others under certain seasonal or structural conditions, which contributes to uncertainty in predictions.

Variable importance

The variable importance plot for the final XGB model (Figure 5) reveals that spectral indices and selected Sentinel-2 bands were the most

influential predictors for tree species classification. Among these, the multispectral ratio vegetation index (RVI_m) had the highest contribution, followed closely by Sentinel-2 band 11 (B11) and the enhanced vegetation index (EVI). These variables provided significant gains in predictive performance, particularly during spring and summer, suggesting that seasonal phenological differences play a key role in distinguishing tree species. Other important optical bands in the top ten included B7, B4, B8, and B12, which also showed strong contributions across multiple seasons, especially spring and summer. The VV polarization from Sentinel-1 data and the radar vegetation index (RVI_r) were also among the top ten contributors, indicating the added value of radar-derived variables in complementing optical data, especially in less optimal atmospheric conditions or for detecting canopy structure. Vegetation indices and spectral bands from autumn and winter generally showed lower overall importance but still contributed meaningfully to predictors like EVI, B4, B8, and radar-derived indices such as RVI_r and VH, indicating that incorporating year-round observations enhances model robustness. The contribution of winter data, while lower overall, was still visible for key indices like EVI and RVI_r . This likely reflects their utility in identifying evergreen species such as Norway spruce and Scots pine, which maintain spectral and structural signatures during the dormant season. In contrast to the optical and radar data, auxiliary variables such as canopy height (CHM), slope, elevation (DEM), aspect, and topographic wetness (TWI) had relatively low importance

scores. Among them, CHM was the most influential, though still much less so than the leading spectral and backscatter predictors. This suggests that while elevation and terrain-based predictors offer some explanatory power, they play a secondary role compared to spectral and radar information in this study area.

Comparison with official statistics

Comparison between the tree species area estimates from the final XGB model and official data from the Swedish Forest Statistics (Riksskogstaxeringen 2024) is shown in Figure 6. Across all the six counties that cover the study area – Blekinge, Halland, Jönköping, Kalmar, Kronoberg, and Skåne – the model's predictions show strong agreement with the reference statistics, as indicated by high Pearson correlation coefficient ($r = 0.96$, $P < 0.001$). This suggests that the model not only performs well at the pixel and plot level but also scales effectively to broader regional assessments. Most counties exhibited high correlation ($r \geq 0.94$) and statistically significant relationships ($P < 0.001$) between the mapped and reported species cover, particularly in Jönköping, Kronoberg, and Blekinge, where Pearson's correlation values were the highest.

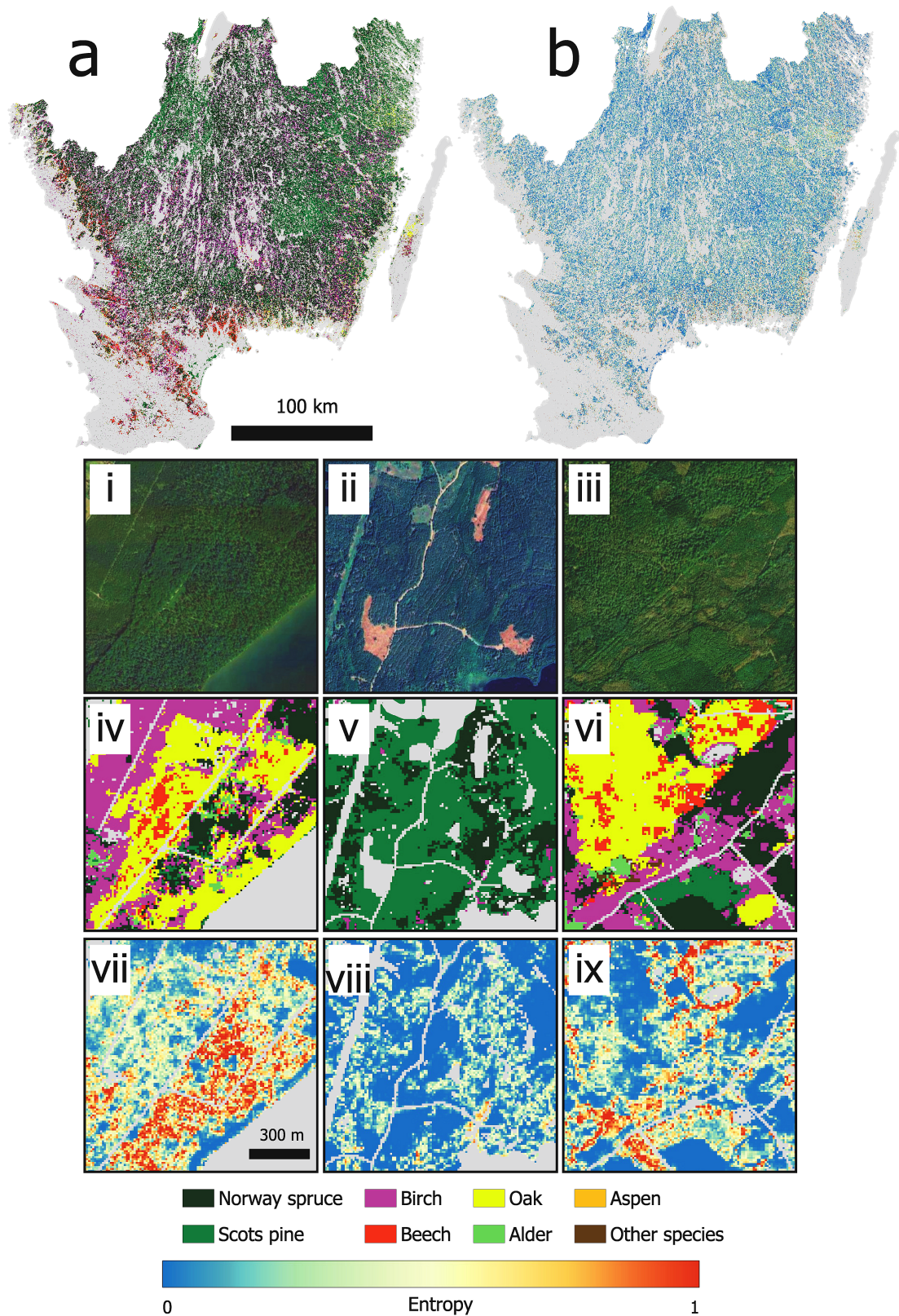
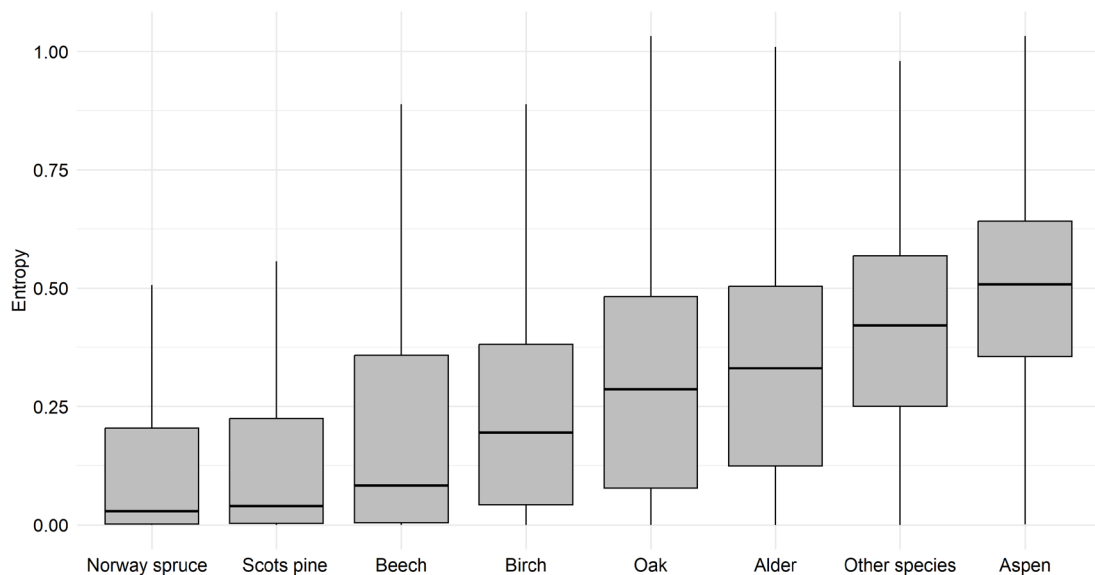


Figure 3. Final tree species classification (a) and the entropy-based uncertainty map (b). The six stacked panels show map details for the classification and uncertainty for: part of a ~200-year-old oak forest at Visingsö in Jönköping (i, iv, vii); a typical Scots pine and Norway spruce dominated production forest in Kronoberg (ii, v, vii); a nemoral forest in Skåne made up of a mosaic of stands comprising different tree species (iii, vi, ix). Entropy-based uncertainty values range from 0 (low uncertainty / high confidence, one class dominates) to 1 (high uncertainty / low confidence, probabilities evenly spread across classes).

Table 2. Performance metrics of the final XGB map based on the independent validation dataset.

Tree Species Class	Performance Metrics				
	Recall <i>Producer's Accuracy</i>	Precision <i>User's Accuracy</i>	Omission Error	Commission Error	F1 Score
Norway spruce	0.846	0.806	0.154	0.193	0.826
Scots pine	0.829	0.831	0.171	0.169	0.830
Birch	0.849	0.853	0.151	0.147	0.851
Beech	0.936	0.919	0.063	0.081	0.928
Oak	0.868	0.880	0.132	0.120	0.874
Alder	0.663	0.788	0.336	0.212	0.721
Aspen	0.764	0.928	0.235	0.071	0.839
Other species	0.661	0.769	0.338	0.231	0.711
Mean \pm StdDev	0.802 \pm 0.09	0.847 \pm 0.05	0.197 \pm 0.09	0.153 \pm 0.05	0.823 \pm 0.07

Overall accuracy = 85%
Matthews correlation coefficient = 0.81

**Figure 4.** Boxplots showing the distribution of classification uncertainty, measured as entropy, across tree species classes in the final XGB model. Lower entropy values indicate higher model confidence in assigning a given class. Species with higher variability and median entropy values, such as aspen and ‘other species’, reflect greater prediction uncertainty, while species like Norway spruce and Scots pine exhibit confident classifications.

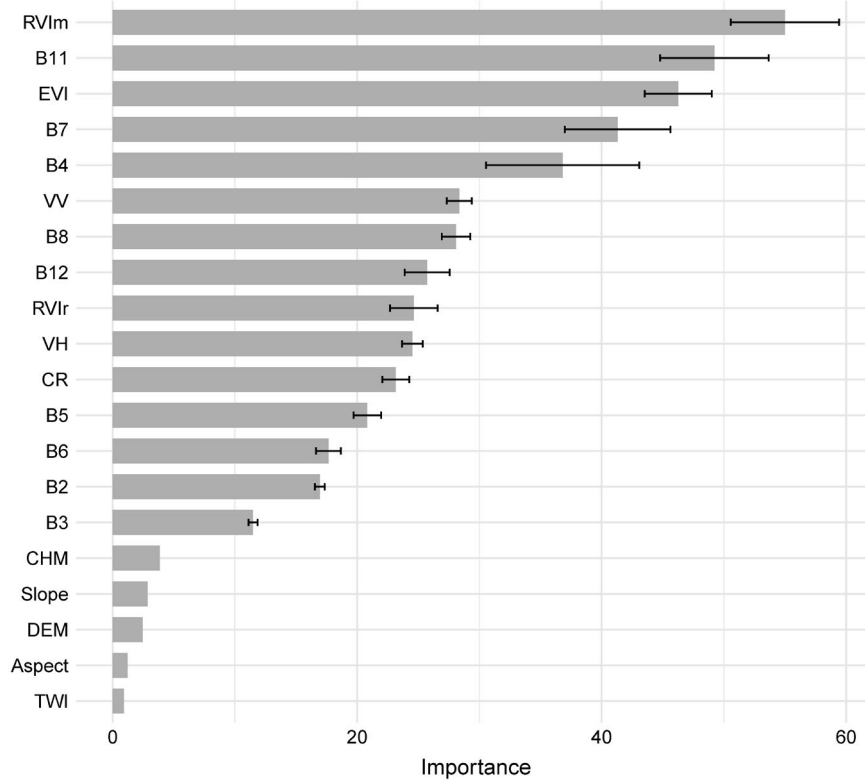


Figure 5. Variable importance scores from the XGB model, aggregated using total gain. This metric reflects how much each predictor variable contributes to improving the model’s predictions by reducing the difference between predicted and actual tree species. Higher values indicate more influential variables. Error bars represent the variability of each variable’s importance across seasons.

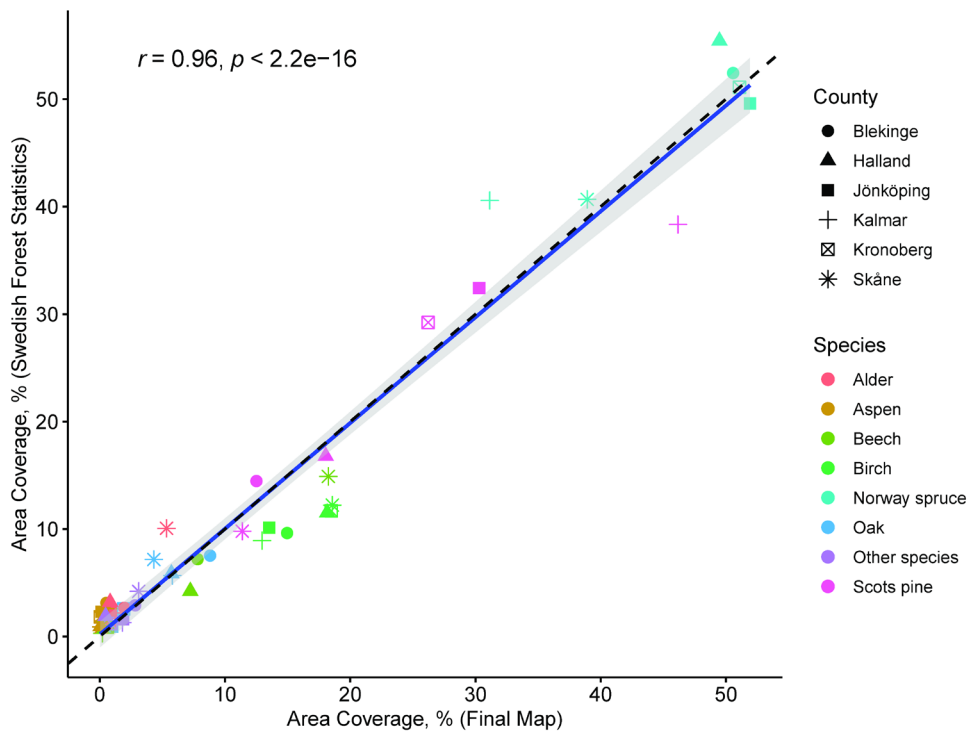


Figure 6. Comparison of the mapped percent cover of the tree species with the official Swedish forest statistics (Riksskogstaxeringen 2024).

Discussion

Mapping tree species across large areas has become increasingly feasible due to advancements in remote sensing technologies and data analysis methods and is an active area of research (Pu 2021; Immitzer and Atzberger 2023). This study provides a robust demonstration of how the complementary use of Sentinel-1 radar, Sentinel-2 multispectral data, and auxiliary variables can enable detailed, spatially continuous mapping of dominant tree species across southern Sweden, with high predictive accuracy and quantifiable uncertainty. We achieved an overall classification accuracy of 85% ($F1 = 0.82$) and strong agreement with official forest statistics ($r = 0.96$) using a classification model based on extreme gradient boosting (XGB), trained and validated with field-based data from the Swedish National Forest Inventory (NFI). These results are broadly consistent with previous work in European forests (Blickensdörfer et al. 2024; Grabska-Szwagrzyk et al. 2024; Breidenbach et al. 2021) that demonstrated the strength of satellite time series for distinguishing dominant species. However, this study extends earlier findings by introducing an entropy-based, pixel-level uncertainty layer to measure model confidence and complement the discrete classification map.

The entropy-based uncertainty map (Figure 3 b) revealed clear species-specific differences in model confidence that closely mirrored the classification performance metrics. Species with high F1 scores such as beech ($F1 = 0.93$), Norway spruce ($F1 = 0.83$), and Scots pine ($F1 = 0.83$) also exhibited low median entropy values (Figure 4). These species likely benefit from distinct spectral-temporal signatures, relatively small intra-species variability of the remote sensing signal, and sufficient representation in the training data. In contrast, species such as alder ($F1 = 0.72$) and the aggregated ‘other species’ class ($F1 = 0.71$) had the highest uncertainty values, reflected in both wider interquartile ranges and higher medians in the entropy distribution. This pattern aligns with their relatively lower precision and recall scores, suggesting that the model struggled to reliably distinguish these classes, likely due to greater spectral overlap, more heterogeneous stand composition, or limited training samples. Lu et al. (2022) applied entropy to evaluate uncertainty in

upscaled land cover maps. Their study showed that entropy effectively captures categorical heterogeneity and highlights spatially variable uncertainty, particularly along class boundaries. Higher entropy values were associated with more ambiguous or underrepresented classes, which supports our interpretation that it provides complementary information to accuracy metrics. This is further supported by Peters et al. (2009) who used entropy to assess prediction uncertainty in vegetation distribution models. Their results showed a clear relationship between entropy values and classification uncertainty, with high entropy corresponding to ambiguous predictions, often due to uncertainty caused by input data limitations or species clustering. This reinforces our finding that entropy is not only a reflection of model performance but also a valuable diagnostic for evaluating confidence in predictions, helping to identify areas and species where additional scrutiny is needed.

The strong performance across dominant tree species such as beech, Norway spruce, Scots pine, and birch suggests that the model successfully captured key phenological and structural signatures using seasonal composites. Species with distinct seasonal dynamics, such as beech (a deciduous tree with strong spring and autumn spectral transitions), showed very high classification certainty and F1 scores above 0.9. Conversely, uncertainty and classification errors were higher for rarer species like alder and the aggregated ‘other species’ class, consistent with prior findings that rare or mixed-species stands introduce confusion (Fassnacht et al. 2016; Grabska-Szwagrzyk et al. 2024). Figure 4 further supports this, showing clear gradients in entropy across species classes, reinforcing the idea that class rarity and within-class spectral variability are key determinants of model uncertainty. The challenge of within-class spectral variability is well-documented in large-scale forest classification, where differences in canopy structure, site conditions, and background signals often lead to increased intra-species variability of the remote sensing signals and classification errors (Fassnacht et al. 2016). We trained a single model using a diverse set of features, including vegetation indices, radar cross-polarizations, and seasonal composites, which resulted in higher model confidence for well-represented species. This

supports the idea that even with a diverse set of features, sufficient training data are required for machine learning algorithms to capture consistent spectral behaviour and structural traits to enhance the classification reliability of tree species.

Classes with lower representation in the training data, such as aspen ($n = 203$) and the heterogeneous ‘other species’ group ($n = 661$), were more prone to misclassification and exhibited higher uncertainty. This is in line with earlier studies that highlight the sensitivity of classification accuracy to reference data imbalance (He and Garcia 2009), particularly for rare or spectrally ambiguous species (Fassnacht et al. 2016). We attempted to address this issue by applying class weighting within the XGB model, which improved the average F1 score compared to other techniques such as down-sampling. This was done by manipulating the *sample_weight* parameter in XGB to assign different weights to individual training samples, influencing how much each sample contributes to the model's loss function and gradient computation during training. The approach should be useful in scenarios like handling class imbalance by giving higher weights to minority class samples to prevent the model from being biased toward the majority class (Chen et al. 2025; Liu and Zhou 2013; Ferrario and Hämmerli 2019). However, the entropy-based uncertainty revealed that these minority classes continued to pose challenges. For example, aspen had high precision (0.93), moderate recall (0.76), and a relatively high median entropy (0.51 ± 0.20) despite addressing class imbalance. This suggests that while the model was selective and usually correct when predicting aspen, it remained uncertain in many of these predictions. The high entropy suggests feature overlap with similar deciduous species (e.g., birch or alder), making it difficult for the model to confidently separate aspen despite weighting adjustments. Thus, despite model-level interventions, limitations in spectral separability and training sample representativeness continue to constrain model performance for underrepresented classes.

The variable importance analysis (Figure 5) highlights the critical role of optical predictors in distinguishing tree species across the study area, with results largely consistent with other remote

sensing studies in European forests (Hemmerling, Pflugmacher, and Hostert 2021; Grabska et al. 2019). Among the Sentinel-2 variables, shortwave infrared (SWIR) band 11 and vegetation indices such as the multispectral ratio vegetation index (RVIm) and enhanced vegetation index (EVI) emerged as particularly influential. The high importance of SWIR (Band 11) can be attributed to its sensitivity to canopy moisture content and leaf internal structure (Lukeš et al. 2013), both of which vary across species due to differences in water retention strategies, leaf morphology, and wood anatomy (Ustin and Gamon 2010). Similarly, EVI and RVIm, which are sensitive to canopy greenness have been shown to capture key phenological and structural attributes that differentiate broadleaf and coniferous species (Peng et al. 2017; Gao et al. 2023). These indices are particularly responsive during leaf-on periods in spring and summer, which is reflected in their seasonal contribution patterns.

Radar-based variables derived from Sentinel-1 also played an important role, with VV backscatter and the radar vegetation index (RVIr) ranking among the top ten predictors. The VV polarization is sensitive to canopy surface roughness and vertical structure, making it particularly useful for identifying structurally complex conifers such as spruce and pine (Bjerreskov, Nord-Larsen, and Fensholt 2021). Radar backscatter retains sensitivity to canopy microstructure during the winter (Dostálová et al. 2021), which may account for the relatively low ranking of winter-season optical variables in our analysis. The inclusion of RVIr, which integrates VV and VH backscatter, has been shown to capture differences in volume scattering and canopy density, traits that are especially relevant in mixed stands or areas with overlapping crown layers (Schellenberg et al. 2023; Hu et al. 2024). This interaction between spectral and structural information highlights the value of integrating radar and optical data for more accurate species classification, particularly in forested areas with spectrally similar species (Mngadi et al. 2021; Bjerreskov, Nord-Larsen, and Fensholt 2021).

Seasonally aggregated variable importance scores showed statistically significant difference in predictive information across seasons ($p = 0.0016$). Imagery acquired during periods of active canopy development, i.e. Spring (MAM) and Summer

(JJA), provided the highest average importance, reflecting the increased spectral and structural differentiation between species during leaf-out and peak growth stages. Autumn (SON), corresponding to the senescence phase, yielded intermediate importance scores, while Winter (DJF) – characterised by leaf-off conditions and reduced photosynthetic activity – contributed the least. This reinforces the importance of phenological timing and highlights the value of seasonally imagery tree species classification.

Although optical and radar predictors dominated the variable importance rankings, geomorphometric variables such as elevation, slope, aspect, and topographic wetness index (TWI) contributed less to model performance. However, canopy height, derived from GEDI-based relative height profiles, showed moderate influence, which is likely due to its ability to differentiate species with characteristic growth forms (Torresani et al. 2023; Zhang et al. 2025), such as tall broadleaf species like beech. Canopy height has been shown to be a useful in predicting tree species diversity, as it integrates ecological dynamics, competition, and habitat variability that are crucial for characterizing species patterns within forested landscapes (Zhang, Wang, et al. 2022; Zhang et al. 2025).

The comparison between mapped species coverage and official forest statistics from the Swedish government (Figure 6) shows strong overall agreement, but some regional discrepancies are evident. In particular, ‘other species’ and alder tend to be slightly overestimated in counties such as Kalmar and Skåne, while species like birch are marginally underestimated in Kronoberg and Halland. These deviations, although modest in magnitude, likely reflect several interacting sources of classification uncertainty. First, spectral similarity among broadleaf species (Fassnacht et al. 2016), such as alder, birch, and aspen, can lead to confusion in the classifier as these species often share similar phenological profiles and canopy structure, particularly when imaged at 10-meter resolution. Second, official statistics are often based on stand-level inventory data that may aggregate or apportion species differently than pixelwise satellite classification (Barrett et al. 2016). For example, mixed stands with co-dominant broadleaf species may be recorded under

a single dominant species in the inventory, while the classifier distributes class labels on a per-pixel basis, potentially resulting in discrepancies in aggregate cover estimates. Third, limitations in spatial resolution and canopy penetration can lead to underrepresentation of species present in the sub-canopy or in structurally complex stands (Dalponte and Coomes 2016). This is especially relevant for species like birch that may occur as a secondary canopy layer beneath taller spruce or pine, which dominate the spectral signal in much of the study area. Despite these challenges, the high degree of alignment across counties confirms the map’s overall reliability and suggests that most deviations can be attributed to predictable sources of ecological and remote sensing complexity rather than model failure.

The strong correlation ($r = 0.96$) between the mapped species cover and official forest statistics highlights that aggregated area estimates are less sensitive to localised classification errors. Whereas pixel-level metrics penalise each misclassification equally, even when confusion is among spectrally similar or spatially adjacent species, area-based statistics smooth out many of these inconsistencies. For example, if some pixels of birch are misclassified as alder, but alder pixels are also occasionally misclassified as birch, the aggregate area estimates for both species may still remain close to their true values at the county level. This effect is particularly relevant in southern Sweden, where species like birch, alder, and aspen often co-occur and may be spectrally similar, especially at 10 m resolution. Similarly, Breidenbach et al. (2021) demonstrated that Sentinel-2-based maps of dominant tree species in Norway showed strong agreement with forest inventory data. While pixel-level accuracy varied locally, aggregated species area estimates at the national level showed only modest correction requirements and resulted in precision gains of up to 50% compared to field-based estimates alone.

Furthermore, differences in how species dominance is interpreted, per pixel in remote sensing versus per stand in field-based inventories, can lead to small discrepancies that likely do not have significant impacts on total area estimates. As noted by Wulder et al. (2020) in their Landsat-based assessment of Canadian forest area, such

structural and definitional mismatches between field inventories and raster-based classifications can still yield high agreement when results are aggregated spatially. Their study reported 84% spatial agreement between Landsat-derived and NFI-derived forest area classifications, and only 3% difference in total forest area at the national level, albeit local classification discrepancies were non-negligible.

Conclusions

Accurate, spatially explicit information on forest composition is increasingly vital for managing biodiversity, monitoring ecological change, and informing sustainable forest policy. This study presents a national-scale approach for mapping dominant tree species across southern Sweden using freely available Sentinel-1 and Sentinel-2 data in combination with topographic predictors and field observations from the Swedish National Forest Inventory. The classification model, based on extreme gradient boosting with Bayesian optimization, achieved high accuracy, with F1 scores exceeding 0.8 for most species. Our mapped species distributions closely matched official forest statistics, with a correlation coefficient of 0.96 at the county level, despite modest pixel-level uncertainty. Much of this uncertainty was concentrated in species with limited training data or greater spectral overlap, such as alder and aspen.

Entropy-based uncertainty was used to quantify classification confidence at the pixel level, which provided a practical tool for assessing spatial variation in model reliability. Our model identified key predictors capturing species-specific differences in seasonal spectral response and canopy structure. Features derived from the shortwave infrared region and vegetation indices contributed most to classification accuracy, while radar-derived metrics provided complementary information on forest structure. The inclusion of these features enabled the model to capture both coniferous and broadleaf species patterns across the ecologically heterogeneous landscapes of southern Sweden.

As forest monitoring needs grow in response to climate change, biodiversity loss, and policy demands, the remote sensing workflow developed

in this study provides a scalable method for producing species-level forest maps with integrated uncertainty estimates. The approach is compatible with operational monitoring requirements and supports current EU policy efforts to improve the spatial and temporal resolution of forest data, including the proposed Forest Monitoring Law and the Nature Restoration Law. This study demonstrates that remote sensing can contribute consistent, spatially detailed information on forest composition suitable for both research and decision-making contexts.

Acknowledgements

The authors thank the Swedish National Forest Inventory for collecting and supplying the data that forms an integral part of this study. This study is funded by the Swedish National Space Agency and is a contribution to the Strategic Research Area ‘Biodiversity and Ecosystem Services in a Changing Climate’ (BECC) funded by the Government of Sweden. Open access funding was provided by Lund University.

References

- Atzberger, C., Zeug, P., Defourny, L., Aragão, L., Hammarström, and M. Immitzer. 2020. ‘Monitoring of forests through remote sensing’. In: Directorate-General for Environment: European Commission.
- Barrett, Frank, Ronald E. McRoberts, Erkki Tomppo, Emil Cienciala, and Lars T. Waser. 2016. ‘A questionnaire-based review of the operational use of remotely sensed data by national forest inventories.’ *Remote Sensing of Environment* 174:279-289. <https://doi.org/https://doi.org/10.1016/j.rse.2015.08.029>.
- Besic, N., N. Picard, C. Vega, J. D. Bontemps, L. Hertzog, J. P. Renaud, F. Fogel, et al. 2025. ‘Remote-sensing-based forest canopy height mapping: some models are useful, but might they provide us with even more insights when combined?’ *Geosci. Model Dev.* 18 (2):337-359. <https://doi.org/10.5194/gmd-18-337-2025>.
- Bjerrreskov, Kristian Skau, Thomas Nord-Larsen, and Rasmus Fensholt. 2021. ‘Classification of Nemoral Forests with Fusion of Multi-

- Temporal Sentinel-1 and 2 Data.’ *Remote Sensing* 13 (5):950.
- Blickensdorfer, Lukas, Katja Oehmichen, Dirk Pflugmacher, Birgit Kleinschmit, and Patrick Hostert. 2024. ‘National tree species mapping using Sentinel-1/2 time series and German National Forest Inventory data.’ *Remote Sensing of Environment* 304:114069.
<https://doi.org/https://doi.org/10.1016/j.rse.2024.114069>.
- Breidenbach, Johannes, Lars T. Waser, Misganu Debella-Gilo, Johannes Schumacher, Johannes Rahlf, Marius Hauglin, Stefano Puliti, and Rasmus Astrup. 2021. ‘National mapping and estimation of forest area by dominant tree species using Sentinel-2 data.’ *Canadian Journal of Forest Research* 51 (3):365-379.
<https://doi.org/10.1139/cjfr-2020-0170>.
- Chen, T, T He, M Benesty, V Khotilovich, Y Tang, H Cho, K Chen, et al. 2025. ‘xgboost: Extreme Gradient Boosting.’ In.
<https://github.com/dmlc/xgboost>: R package version 3.0.0.1
- Chen, Tianqi, and Carlos Guestrin. 2016. ‘XGBoost: A Scalable Tree Boosting System.’ In *Proceedings of the 22nd ACM SIGKDD International Conference on Knowledge Discovery and Data Mining*, 785–794. San Francisco, California, USA: Association for Computing Machinery.
- Creed, Irena F., Marian Weber, Francesco Accatino, and David P. Kreuzweiser. 2016. ‘Managing Forests for Water in the Anthropocene—The Best Kept Secret Services of Forest Ecosystems.’ *Forests* 7 (3):60.
- Dalponte, Michele, and David A. Coomes. 2016. ‘Tree-centric mapping of forest carbon density from airborne laser scanning and hyperspectral data.’ *Methods in Ecology and Evolution* 7 (10):1236-1245.
<https://doi.org/https://doi.org/10.1111/2041-210X.12575>.
- Dlamini, Cliff S. 2019. ‘Contribution of Forest Ecosystem Services Toward Food Security and Nutrition.’ In *Zero Hunger*, edited by Walter Leal Filho, Anabela Marisa Azul, Luciana Brandli, Pinar Gökcin Özuyar and Tony Wall, 1-18. Cham: Springer.
- Dostálová, Alena, Mait Lang, Janis Ivanovs, Lars T. Waser, and Wolfgang Wagner. 2021. ‘European Wide Forest Classification Based on Sentinel-1 Data.’ *Remote Sensing* 13 (3):337.
- Dostálová, Alena, Wolfgang Wagner, Milutin Milenković, and Markus Hollaus. 2018. ‘Annual seasonality in Sentinel-1 signal for forest mapping and forest type classification.’ *International Journal of Remote Sensing* 39 (21):7738-7760.
<https://doi.org/10.1080/01431161.2018.1479788>.
- Dubayah, Ralph, James Bryan Blair, Scott Goetz, Lola Fatoyinbo, Matthew Hansen, Sean Healey, Michelle Hofton, et al. 2020. ‘The Global Ecosystem Dynamics Investigation: High-resolution laser ranging of the Earth’s forests and topography.’ *Science of Remote Sensing* 1:100002.
<https://doi.org/https://doi.org/10.1016/j.srs.2020.100002>.
- European Commission. 2021. ‘New EU Forest Strategy for 2030.’ In.
———. ‘Commission proposes comprehensive monitoring to improve resilience of European forests.’
https://ec.europa.eu/commission/presscorner/detail/en/ip_23_5909.
- Farhadur Rahman, Md, Yusuke Onoda, and Kaoru Kitajima. 2022. ‘Forest canopy height variation in relation to topography and forest types in central Japan with LiDAR.’ *Forest Ecology and Management* 503:119792.
<https://doi.org/https://doi.org/10.1016/j.foreco.2021.119792>.
- Fassnacht, Fabian Ewald, Hooman Latifi, Krzysztof Stereńczak, Aneta Modzelewska, Michael Lefsky, Lars T. Waser, Christoph Straub, and Aniruddha Ghosh. 2016. ‘Review of studies on tree species classification from remotely sensed data.’ *Remote Sensing of Environment* 186:64-87.
<https://doi.org/https://doi.org/10.1016/j.rse.2016.08.013>.
- Ferrario, Andrea, and Roger Hämmerli. 2019. ‘On Boosting: Theory and Applications.’ In.: ETH Zurich, Mobiliar Lab for Analytics.

- Fridman, Jonas, Sören Holm, Mats Nilsson, Per Nilsson, Anna Hedström Ringvall, and Göran Ståhl. 2014. *Adapting National Forest Inventories to changing requirements – the case of the Swedish National Forest Inventory at the turn of the 20th century*. Vol. 48.
- Fridman, Jonas, and Bertil Westerlund. 2016. 'Swedish National Forest Inventory.' In *National Forest Inventories: Assessment of Wood Availability and Use*, edited by Claude Vidal, Iciar A. Alberdi, Laura Hernández Mateo and John J. Redmond, 769-782. Cham: Springer International Publishing.
- Gao, Si, Run Zhong, Kai Yan, Xuanlong Ma, Xinkun Chen, Jiabin Pu, Sicong Gao, Jianbo Qi, Gaofei Yin, and Ranga B. Myneni. 2023. 'Evaluating the saturation effect of vegetation indices in forests using 3D radiative transfer simulations and satellite observations.' *Remote Sensing of Environment* 295:113665. <https://doi.org/https://doi.org/10.1016/j.rse.2023.113665>.
- Gorelick, Noel, Matt Hancher, Mike Dixon, Simon Ilyushchenko, David Thau, and Rebecca Moore. 2017. 'Google Earth Engine: Planetary-scale geospatial analysis for everyone.' *Remote Sensing of Environment* 202:18-27. <https://doi.org/https://doi.org/10.1016/j.rse.2017.06.031>.
- Grabska-Szwagrzyk, E., D. Tiede, M. Sudmanns, and J. Kozak. 2024. 'Map of forest tree species for Poland based on Sentinel-2 data.' *Earth Syst. Sci. Data* 16 (6):2877-2891. <https://doi.org/10.5194/essd-16-2877-2024>.
- Grabska, Ewa, David Frantz, and Katarzyna Ostapowicz. 2020. 'Evaluation of machine learning algorithms for forest stand species mapping using Sentinel-2 imagery and environmental data in the Polish Carpathians.' *Remote Sensing of Environment* 251:112103. <https://doi.org/https://doi.org/10.1016/j.rse.2020.112103>.
- Grabska, Ewa, Patrick Hostert, Dirk Pflugmacher, and Katarzyna Ostapowicz. 2019. 'Forest Stand Species Mapping Using the Sentinel-2 Time Series.' *Remote Sensing* 11 (10):1197.
- Hakkenberg, Christopher R., Conghe Song, Robert K. Peet, and Peter S. White. 2016. 'Forest structure as a predictor of tree species diversity in the North Carolina Piedmont.' *Journal of Vegetation Science* 27 (6):1151-1163. <https://doi.org/https://doi.org/10.1111/jvs.12451>.
- Hawker, Laurence, Peter Uhe, Luntadila Paulo, Jeison Sosa, James Savage, Christopher Sampson, and Jeffrey Neal. 2022. 'A 30 m global map of elevation with forests and buildings removed.' *Environmental Research Letters* 17 (2):024016. <https://doi.org/10.1088/1748-9326/ac4d4f>.
- He, H., and E. A. Garcia. 2009. 'Learning from Imbalanced Data.' *IEEE Transactions on Knowledge and Data Engineering* 21 (9):1263-1284. <https://doi.org/10.1109/TKDE.2008.239>.
- Head, Tim, Manoj Kumar, Holger Nahrstaedt, Gilles Louppe, and Iaroslav Shcherbatyi. 2021. 'scikit-optimize/scikit-optimize (v0.9.0).' *Zenodo*.
- Hemmerling, Jan, Dirk Pflugmacher, and Patrick Hostert. 2021. 'Mapping temperate forest tree species using dense Sentinel-2 time series.' *Remote Sensing of Environment* 267:112743. <https://doi.org/https://doi.org/10.1016/j.rse.2021.112743>.
- Hermosilla, Txomin, Alex Bastyr, Nicholas C. Coops, Joanne C. White, and Michael A. Wulder. 2022. 'Mapping the presence and distribution of tree species in Canada's forested ecosystems.' *Remote Sensing of Environment* 282:113276. <https://doi.org/https://doi.org/10.1016/j.rse.2022.113276>.
- Hu, Xueqian, Li Li, Jianxi Huang, Yelu Zeng, Shuo Zhang, Yiran Su, Yujiao Hong, and Zixiang Hong. 2024. 'Radar vegetation indices for monitoring surface vegetation: Developments, challenges, and trends.' *Science of The Total Environment* 945:173974. <https://doi.org/https://doi.org/10.1016/j.scitotenv.2024.173974>.

- Huang, Jiapeng, and Xiaozhu Yang. 2025. 'Evaluation and improvement of the vertical accuracy of the global open DEM under forest environment.' *Geocarto International* 40 (1):2453024. <https://doi.org/10.1080/10106049.2025.2453024>.
- Huete, A., K. Didan, T. Miura, E. P. Rodriguez, X. Gao, and L. G. Ferreira. 2002. 'Overview of the radiometric and biophysical performance of the MODIS vegetation indices.' *Remote Sensing of Environment* 83 (1):195-213. [https://doi.org/https://doi.org/10.1016/S0034-4257\(02\)00096-2](https://doi.org/https://doi.org/10.1016/S0034-4257(02)00096-2).
- Immitzer, Markus, and Clement Atzberger. 2023. 'Tree Species Diversity Mapping—Success Stories and Possible Ways Forward.' *Remote Sensing* 15 (12):3074.
- Lang, Nico, Walter Jetz, Konrad Schindler, and Jan Dirk Wegner. 2023. 'A high-resolution canopy height model of the Earth.' *Nature Ecology & Evolution* 7 (11):1778-1789. <https://doi.org/10.1038/s41559-023-02206-6>.
- Laurin, Gaia Vaglio, Saverio Francini, Daniele Penna, Giulia Zuecco, Gherardo Chirici, Ethan Berman, Nicholas C. Coops, et al. 2022. 'SnowWarp: An open science and open data tool for daily monitoring of snow dynamics.' *Environmental Modelling & Software* 156:105477. <https://doi.org/https://doi.org/10.1016/j.envsoft.2022.105477>.
- Lechner, Michael, Alena Dostálová, Markus Hollaus, Clement Atzberger, and Markus Immitzer. 2022. 'Combination of Sentinel-1 and Sentinel-2 Data for Tree Species Classification in a Central European Biosphere Reserve.' *Remote Sensing* 14 (11):2687.
- Liang, Jingjing, Thomas W. Crowther, Nicolas Picard, Susan Wiser, Mo Zhou, Giorgio Alberti, Ernst-Detlef Schulze, et al. 2016. 'Positive biodiversity-productivity relationship predominant in global forests.' *Science* 354 (6309):aaf8957. <https://doi.org/doi:10.1126/science.aaf8957>.
- Liu, Xiaojuan, Stefan Trogisch, Jin-Sheng He, Pascal A. Niklaus, Helge Bruelheide, Zhiyao Tang, Alexandra Erfmeier, et al. 2018. 'Tree species richness increases ecosystem carbon storage in subtropical forests.' *Proceedings of the Royal Society B: Biological Sciences* 285 (1885):20181240. <https://doi.org/doi:10.1098/rspb.2018.1240>.
- Liu, Xu-Ying, and Zhi-Hua Zhou. 2013. 'Ensemble Methods for Class Imbalance Learning.' In *Imbalanced Learning*, 61-82.
- Louis, Jérôme, Vincent Debaecker, Bringfried Pflug, Magdalena Main-Knorn, Jakub Bieniarz, Uwe Mueller-Wilm, Enrico Cadau, and Ferran Gascon. 2016. Sentinel-2 Sen2Cor: L2A processor for users. Paper presented at the Proceedings of the Living Planet Symposium 2016, Prague.
- Louis, Jérôme, and L2A Team. 2021. 'Sentinel-2 Level-2A Algorithm Theoretical Basis Document.' In.: European Space Agency.
- Lu, Yunduo, Sun Peijun, Linghu Linna, and Meng and Zhang. 2022. 'Uncertainty evaluation approach based on Shannon entropy for upscaled land use/cover maps.' *Journal of Land Use Science* 17 (1):648-657. <https://doi.org/10.1080/1747423X.2022.2141364>.
- Lukeš, Petr, Stenberg Pauline, Rautiainen Miina, Mõttus Matti, and Kalle M. and Vanhatalo. 2013. 'Optical properties of leaves and needles for boreal tree species in Europe.' *Remote Sensing Letters* 4 (7):667-676. <https://doi.org/10.1080/2150704X.2013.782112>.
- Lundström, Anders, and Per-Erik Wikberg. 2017. 'Sweden.' In *Forest Inventory-based Projection Systems for Wood and Biomass Availability*, edited by Susana Barreiro, Mart-Jan Schelhaas, Ronald E. McRoberts and Gerald Kändler, 289-301. Cham: Springer International Publishing.
- Marsh, Christopher B., Phillip Harder, and John W. Pomeroy. 2023. 'Validation of FABDEM, a global bare-earth elevation model, against UAV-lidar derived elevation in a complex forested mountain catchment.' *Environmental Research Communications* 5 (3):031009. <https://doi.org/10.1088/2515-7620/acc56d>.
- Mngadi, Mthembeni, Odindi John, Peerbhay Kabir, and Onesimo and Mutanga. 2021. 'Examining the effectiveness of Sentinel-1

- and 2 imagery for commercial forest species mapping.’ *Geocarto International* 36 (1):1-12.
<https://doi.org/10.1080/10106049.2019.1585483>.
- Morin, Xavier, Lorenz Fahse, Hervé Jactel, Michael Scherer-Lorenzen, Raúl García-Valdés, and Harald Bugmann. 2018. ‘Long-term response of forest productivity to climate change is mostly driven by change in tree species composition.’ *Scientific Reports* 8 (1):5627.
<https://doi.org/10.1038/s41598-018-23763-y>.
- Morin, Xavier, Lorenz Fahse, Michael Scherer-Lorenzen, and Harald Bugmann. 2011. ‘Tree species richness promotes productivity in temperate forests through strong complementarity between species.’ *Ecology Letters* 14 (12):1211-1219.
<https://doi.org/https://doi.org/10.1111/j.1461-0248.2011.01691.x>.
- Mullissa, Adugna, Andreas Vollrath, Christelle Odongo-Braun, Bart Slagter, Johannes Balling, Yaqing Gou, Noel Gorelick, and Johannes Reiche. 2021. ‘Sentinel-1 SAR Backscatter Analysis Ready Data Preparation in Google Earth Engine.’ *Remote Sensing* 13 (10).
<https://doi.org/10.3390/rs13101954>.
- Nasiri, Vahid, Mirela Beloiu, Ali Asghar Darvishsefat, Verena C. Griess, Carmen Maftai, and Lars T. Waser. 2023. ‘Mapping tree species composition in a Caspian temperate mixed forest based on spectral-temporal metrics and machine learning.’ *International Journal of Applied Earth Observation and Geoinformation* 116:103154.
<https://doi.org/https://doi.org/10.1016/j.jag.2022.103154>.
- Nasirzadehdizaji, Rouhollah, Fusun Balik Sanli, Saygin Abdikan, Ziyadin Cakir, Aliihsan Sekertekin, and Mustafa Ustuner. 2019. ‘Sensitivity Analysis of Multi-Temporal Sentinel-1 SAR Parameters to Crop Height and Canopy Coverage.’ *Applied Sciences* 9 (4):655.
- Osama, Nahed, Zhenfeng Shao, and Mohamed Freeshah. 2023. ‘The FABDEM Outperforms the Global DEMs in Representing Bare Terrain Heights.’ *Photogrammetric Engineering & Remote Sensing* 89 (10):613-624.
- Ottosen, Thor-Bjørn, Geoffrey Petch, Mary Hanson, and Carsten A. Skjøth. 2020. ‘Tree cover mapping based on Sentinel-2 images demonstrate high thematic accuracy in Europe.’ *International Journal of Applied Earth Observation and Geoinformation* 84:101947.
<https://doi.org/https://doi.org/10.1016/j.jag.2019.101947>.
- Pan, Yude, Richard A. Birdsey, Oliver L. Phillips, Richard A. Houghton, Jingyun Fang, Pekka E. Kauppi, Heather Keith, et al. 2024. ‘The enduring world forest carbon sink.’ *Nature* 631 (8021):563-569.
<https://doi.org/10.1038/s41586-024-07602-x>.
- Pearson, Robert Lawrence, and Lee Durward Miller. 1972. Remote mapping of standing crop biomass for estimation of the productivity of the shortgrass prairie, Pawnee National Grasslands, Colorado. Paper presented at the Proceedings of the 8th International Symposium on Remote Sensing of the Environment
- Peh, Kelvin S.-H. , Richard T. Corlett, and Yves Bergeron. 2025. ‘Part 3: Forest Flora and Fauna.’ In *Routledge Handbook of Forest Ecology*, 211 - 339. London: Routledge.
- Peng, Dailiang, Chaoyang Wu, Cunjun Li, Xiaoyang Zhang, Zhengjia Liu, Huichun Ye, Shezhou Luo, Xinjie Liu, Yong Hu, and Bin Fang. 2017. ‘Spring green-up phenology products derived from MODIS NDVI and EVI: Intercomparison, interpretation and validation using National Phenology Network and AmeriFlux observations.’ *Ecological Indicators* 77:323-336.
<https://doi.org/https://doi.org/10.1016/j.ecolind.2017.02.024>.
- Persson, Magnus, Eva Lindberg, and Heather Reese. 2018. ‘Tree Species Classification with Multi-Temporal Sentinel-2 Data.’ *Remote Sensing* 10 (11):1794.
- Peters, Jan, Niko E. C. Verhoest, Roeland Samson, Marc Van Meirvenne, Liesbet Cockx, and Bernard De Baets. 2009. ‘Uncertainty propagation in vegetation distribution

- models based on ensemble classifiers.’ *Ecological Modelling* 220 (6):791-804.
<https://doi.org/https://doi.org/10.1016/j.ecolmodel.2008.12.022>.
- Ploton, Pierre, Frédéric Mortier, Maxime Réjou-Méchain, Nicolas Barbier, Nicolas Picard, Vivien Rossi, Carsten Dormann, et al. 2020. ‘Spatial validation reveals poor predictive performance of large-scale ecological mapping models.’ *Nature Communications* 11 (1):4540.
<https://doi.org/10.1038/s41467-020-18321-y>.
- Preislerová, Zdenka, Corrado Marcenò, Javier Loidi, Gianmaria Bonari, Dariia Borovyk, Rosario G. Gavilán, Valentin Golub, et al. 2024. ‘Structural, ecological and biogeographical attributes of European vegetation alliances.’ *Applied Vegetation Science* 27 (1):e12766.
<https://doi.org/https://doi.org/10.1111/avsc.12766>.
- Pu, Ruiliang. 2021. ‘Mapping Tree Species Using Advanced Remote Sensing Technologies: A State-of-the-Art Review and Perspective.’ *Journal of Remote Sensing* 2021.
<https://doi.org/doi:10.34133/2021/9812624>.
- Raši, Rastislav. 2020. ‘State of Europe’s Forests 2020.’ In.: Ministerial Conference on the Protection of Forests in Europe.
- Rignot, E. J. M., C. L. Williams, J. Way, and L. A. Viereck. 1994. ‘Mapping of forest types in Alaskan boreal forests using SAR imagery.’ *IEEE Transactions on Geoscience and Remote Sensing* 32 (5):1051-1059.
<https://doi.org/10.1109/36.312893>.
- Riksdag. 1979. ‘Skogsvårdslag.’ In 1979:429, 2 § första stycket 2. Sverige: Landsbygds- och infrastrukturdepartementet.
- Riksskogstaxeringen. 2024. ‘Forest Statistics 2024 - Official Statistics of Sweden.’ In.
https://www.slu.se/globalassets/ew/org/centrb/rt/dokument/skogsdata/skogsdata_2024_web.pdf.
- Roberge, J-M., C. Fries, E. Normark, E. Mårald, A. Sténs, C. Sandström, J. Sonesson, C. Appelqvist, and T. Lundmark. 2020. ‘Forest management in Sweden - Current practice and historical background.’ In.: Skogsstyrelsen.
- Roberts, David R., Volker Bahn, Simone Ciuti, Mark S. Boyce, Jane Elith, Gurutzeta Guillera-Aroita, Severin Hauenstein, et al. 2017. ‘Cross-validation strategies for data with temporal, spatial, hierarchical, or phylogenetic structure.’ *Ecography* 40 (8):913-929.
<https://doi.org/https://doi.org/10.1111/ecog.02881>.
- Schadauer, Klemens, Rasmus Astrup, Johannes Breidenbach, Jonas Fridman, Stephan Gräber, Michael Köhl, Kari T. Korhonen, et al. 2024. ‘Access to exact National Forest Inventory plot locations must be carefully evaluated.’ *New Phytologist* 242 (2):347-350.
<https://doi.org/https://doi.org/10.1111/nph.19564>.
- Schellenberg, Konstantin, Thomas Jagdhuber, Markus Zehner, Sören Hese, Marcel Urban, Mikhail Urbazaev, Henrik Hartmann, Christiane Schmuilius, and Clémence Dubois. 2023. ‘Potential of Sentinel-1 SAR to Assess Damage in Drought-Affected Temperate Deciduous Broadleaf Forests.’ *Remote Sensing* 15 (4):1004.
- Seibert, Jan, Johan Stendahl, and Rasmus Sørensen. 2007. ‘Topographical influences on soil properties in boreal forests.’ *Geoderma* 141 (1):139-148.
<https://doi.org/https://doi.org/10.1016/j.geoderma.2007.05.013>.
- Shannon, C. E. 1948. ‘A Mathematical Theory of Communication.’ *Bell System Technical Journal* 27 (3):379-423.
<https://doi.org/https://doi.org/10.1002/j.1538-7305.1948.tb01338.x>.
- Stock, Andy, Edward J. Gregr, and Kai M. A. Chan. 2023. ‘Data leakage jeopardizes ecological applications of machine learning.’ *Nature Ecology & Evolution* 7 (11):1743-1745.
<https://doi.org/10.1038/s41559-023-02162-1>.
- Torresani, Michele, Duccio Rocchini, Alessandro Alberti, Vítězslav Moudrý, Michael Heym, Elisa Thouverai, Patrick Kacic, and Enrico Tomelleri. 2023. ‘LiDAR GEDI derived tree canopy height heterogeneity reveals patterns of biodiversity in forest ecosystems.’ *Ecological Informatics* 76:102082.

- <https://doi.org/https://doi.org/10.1016/j.ecoi.nf.2023.102082>.
- Torresani, Michele, Duccio Rocchini, Ruth Sonnenschein, Marc Zebisch, Heidi C. Hauffe, Michael Heym, Hans Pretzsch, and Giustino Tonon. 2020. 'Height variation hypothesis: A new approach for estimating forest species diversity with CHM LiDAR data.' *Ecological Indicators* 117:106520. <https://doi.org/https://doi.org/10.1016/j.ecoi.ind.2020.106520>.
- Udali, Alberto, Emanuele Lingua, and Henrik J. Persson. 2021. 'Assessing Forest Type and Tree Species Classification Using Sentinel-1 C-Band SAR Data in Southern Sweden.' *Remote Sensing* 13 (16):3237.
- Ustin, Susan L., and John A. Gamon. 2010. 'Remote sensing of plant functional types.' *New Phytologist* 186 (4):795-816. <https://doi.org/https://doi.org/10.1111/j.1469-8137.2010.03284.x>.
- Valavi, Roozbeh, Jane Elith, José J. Lahoz-Monfort, and Gurutzeta Guillera-Arroita. 2019. 'blockCV: An r package for generating spatially or environmentally separated folds for k-fold cross-validation of species distribution models.' *Methods in Ecology and Evolution* 10 (2):225-232. <https://doi.org/https://doi.org/10.1111/2041-210X.13107>.
- Varghese, A. O., and A. K. Joshi. 2015. 'Polarimetric classification of C-band SAR data for forest density characterization.' *Current Science* 108 (1):100-106.
- Varghese, Alappat Ouseph, Arun Suryavanshi, and Asokh Kumar Joshi. 2016. 'Analysis of different polarimetric target decomposition methods in forest density classification using C band SAR data.' *International Journal of Remote Sensing* 37 (3):694-709. <https://doi.org/10.1080/01431161.2015.1136448>.
- Vreugdenhil, Mariette, Claudio Navacchi, Bernhard Bauer-Marschallinger, Sebastian Hahn, Susan Steele-Dunne, Isabella Pfeil, Wouter Dorigo, and Wolfgang Wagner. 2020. 'Sentinel-1 Cross Ratio and Vegetation Optical Depth: A Comparison over Europe.' *Remote Sensing* 12 (20):3404.
- Wang, Qiuping A. 2008. 'Probability distribution and entropy as a measure of uncertainty.' *Journal of Physics A: Mathematical and Theoretical* 41 (6):065004. <https://doi.org/10.1088/1751-8113/41/6/065004>.
- Welle, Torsten, Lukas Aschenbrenner, Kevin Kuonath, Stefan Kirmaier, and Jonas Franke. 2022. 'Mapping Dominant Tree Species of German Forests.' *Remote Sensing* 14 (14):3330.
- White, J. C., M. A. Wulder, G. W. Hobart, J. E. Luther, T. Hermosilla, P. Griffiths, N. C. Coops, et al. 2014. 'Pixel-Based Image Compositing for Large-Area Dense Time Series Applications and Science.' *Canadian Journal of Remote Sensing* 40 (3):192-212. <https://doi.org/10.1080/07038992.2014.945827>.
- Wulder, Michael A, Txomin Hermosilla, Graham Stinson, François A Gougeon, Joanne C White, David A Hill, and Byron P Smiley. 2020. 'Satellite-based time series land cover and change information to map forest area consistent with national and international reporting requirements.' *Forestry: An International Journal of Forest Research* 93 (3):331-343. <https://doi.org/10.1093/forestry/cpaa006>.
- Zhang, Lei, Liu Yang, Jinhua Sun, Qimeng Zhu, Ting Wang, and Hui Zhao. 2025. 'Estimation of Tree Species Diversity in Warm Temperate Forests via GEDI and GF-1 Imagery.' *Forests* 16 (4):570.
- Zhang, Shengmin, Dries Landuyt, Kris Verheyen, and Pieter De Frenne. 2022. 'Tree species mixing can amplify microclimate offsets in young forest plantations.' *Journal of Applied Ecology* 59 (6):1428-1439. <https://doi.org/https://doi.org/10.1111/1365-2664.14158>.
- Zhang, Yicen, Junjie Wang, Zhifeng Wu, Juyuan Lian, Wanhui Ye, and Fangyuan Yu. 2022. 'Tree Species Classification Using Plant Functional Traits and Leaf Spectral Properties along the Vertical Canopy Position.' *Remote Sensing* 14 (24):6227.